

Journal of Materials Chemistry A

Accepted Manuscript



This is an *Accepted Manuscript*, which has been through the Royal Society of Chemistry peer review process and has been accepted for publication.

Accepted Manuscripts are published online shortly after acceptance, before technical editing, formatting and proof reading. Using this free service, authors can make their results available to the community, in citable form, before we publish the edited article. We will replace this *Accepted Manuscript* with the edited and formatted *Advance Article* as soon as it is available.

You can find more information about *Accepted Manuscripts* in the [Information for Authors](#).

Please note that technical editing may introduce minor changes to the text and/or graphics, which may alter content. The journal's standard [Terms & Conditions](#) and the [Ethical guidelines](#) still apply. In no event shall the Royal Society of Chemistry be held responsible for any errors or omissions in this *Accepted Manuscript* or any consequences arising from the use of any information it contains.

ARTICLE

Facile single step synthesis of flowery shape pure/lithium doped 3D iron oxides

Cite this: DOI: 10.1039/x0xx00000x

Rasmita Barik,^a Brajesh Pandey^b, Shashi Anand^a, and Mamata Mohapatra^{*a}Received 00th January 2014,
Accepted 00th January 2014

DOI: 10.1039/x0xx00000x

www.rsc.org/

The shape dependent surface properties of iron oxides are being paid increased attention for many advanced and synergistic applications. The present investigation deals with the preparation of pure and lithiated 3D iron oxide through a simple and single step synthesis route. The nano hierarchical flowers were synthesized by adopting a semi-aqueous ligated system. Here the reagent played a double role for ligation as well as for precipitation. In the absence of lithium, goethite and ferrihydrite phases were formed, whereas formation of a mixture of hematite and ferrihydrite was observed in its presence confirming participation of Li in phase transformation of goethite/ferrihydrite to hematite. With the progress of time evolution of flowery shape nano particles took place. Mössbauer spectroscopy revealed Li ion induced formation of α -Fe₂O₃ phase. Single phase hematite was formed on annealing at 500 °C. Li- doped iron oxide sample has high surface area and has sharp distribution peak centered at 19.13 nm showing homogeneity of the pores. On calcination of the sample at 400 °C, the surface area decreased, however, pore size distribution remained unchanged which was an unusual trend. The annealed sample (500 °C) possessed bimodal (small and large) mesopore distribution. The fluoride adsorption behaviour and magnetic properties of the as synthesized and annealed Li-doped samples have been discussed. Magnetic properties of the samples suggested that incorporation of Li resulted in increase of coercivity due to stabilization of domain. The unique surface behaviour of the present samples can be further examined for other high end applications. The present synthesis strategy has advantage of producing shape controlled, hierarchical materials with tunable surface properties which promises further development of other functional materials.

Introduction

Synthesis and fabrication of shape oriented nano-structured α -FeOOH/Fe₂O₃ through solution routes have been intensively investigated for realizing high-end applications.¹⁻¹¹ Specific application such as semiconductor, catalyst, pigment, chemical sensor, water treatment, and so on are dependent on diverse shaped hematite nanostructures such as nano flower,¹²⁻²¹ nano spindles,¹⁶ nano rods,²² nanowires⁴ and nanotubes.⁵⁻⁶ Among them most efficient strategy to fabricate 3D hierarchical orientation is self-assembling process, in which ordered aggregates are formed. In general, hierarchically self-assembled architectures with designed chemical components and controlled morphologies strongly affect the properties of nanomaterials. Nevertheless, the methods suffer from multistep operations for fabricating colloidal nano crystals before the self-assembly,^{7-9, 23} and removal of intact impurities arising due to use of hard and soft templates such as surfactants, multifunctional organic ligands, polymers, or bio molecules during synthesis steps.^{7-9, 24-30} Synthesis of flowery shaped iron oxide nanoparticles of different phases for advanced applications has been recently attempted applying various approaches.^{12, 17, 31-34} In practical application, it is more desirable to have a simplified self-assembly approach wherein spontaneous aggregation occurs with the formation of primary nano crystals during the synthesis process. A brief summary for the development of flowery iron oxides by various aqueous processing routes is given in supporting Table S1. Developing the flower shaped iron oxide structure with simultaneous incorporation of other metallic

ions through aqueous processing routes for enhanced magnetic and adsorption properties has been scarcely reported. Doping of lithium ions through aqueous route is not reported so far, though it is of great interest due to possible battery applications for construction of galvanic cells of second generation.³⁵ Some work has been reported on solid combustion or mechanical milling of lithium in iron oxide matrix.³⁶⁻³⁷ Iron oxide based electrodes, where only intercalation of Li ions occurs, has been recently found to be promising to design cathodes.³⁸ Incorporation of alkali metal ions resulted in decrease of particle size and increase in the d-spacing between crystal layers.³⁹ This can be utilized for enhancing the targeted applications. Therefore, in the present work; we have proposed to synthesize novel 3D flowerlike mixed iron oxide nano-structures with lithium incorporation in a single step, following a ligand-mediation-precipitation approach. These were preferentially converted to hematite after calcination. It is for the first time such interesting microstructures via a ligand mediated interface is being reported. Considering the current ongoing research on application of metal oxidic surfaces for holding toxin in separation and purification area, we have utilized the as synthesized samples for fluoride removal from aqueous solutions. As is well known, fluoride, being a toxic anion in aqueous media, efforts for its remediation remains to be one of the emerging research fields. Magnetic properties of the synthesized samples have also been evaluated for other advance applications.

Materials and methods

Synthesis of iron oxide 3D-like structures. The chemicals used in the synthesis were: $\text{Fe}(\text{NO}_3)_3 \cdot 6\text{H}_2\text{O}$ (Merck), ethylene glycol mono methyl ether ($\text{CH}_3\text{O} \cdot \text{CH}_2 \cdot \text{CH}_2 \cdot \text{OH}$, EGME) (Merck grade) and lithium hydroxide (LiOH) (Merck). The nano iron oxide precursors were prepared using a simple ligand mediation precipitation approach. In a typical procedure, 50 mL of 0.1 M ferric nitrate solution was taken in a three necked flask attached with a condenser, thermometer and a pH meter (electrode). 150 mL of 0.2 M stock solution of EGME was added with continuous stirring for 10 min to obtain a homogeneous solution. It acts both as ligand and solvent. For preparing Li doped sample, 10 mL of 0.1M lithium hydroxide solution was added. The contents with/ without lithium were heated to 80°C for 3 h. The obtained precipitates were separated by centrifuging and rinsing several times using distilled water and acetone. Finally the products were dried at room temperature. Calcination was carried out in air in an electrical furnace at 400 and 500°C. For chemical analysis, weighed amount of samples were digested in 0.1N HCL and the desired volume was makeup followed by dilution. Iron was analyzed by atomic absorption spectroscopy as well as by volumetric method using barium diphenylamine sulphonate (BDAS) as the indicator.⁴⁰ Lithium was analyzed by ICP-OES (Inductively Coupled Plasma- optical emission spectroscopy), Optima-2100DV, Perkin Elmer.

Characterization. The absorption spectra were taken by Perkin Elmer Lambda-35 UV-Visible Spectrophotometer. Pure isopropyl alcohol (i-PrOH) was used as the blank reference solution. 250 μL of the reaction mixture was taken out from the reaction mixture and mixed with 5 mL of i-PrOH at room temperature and sonicate for 5 minutes. This solution was used immediately to measure the UV-visible absorption for the iron oxide particles. The particle size of the prepared samples is analysed by a particle size analyzer (Microtrac – Zetac). The crystal structures of the samples were studied by X-ray diffraction (XRD) using an automated XRD, Siemens D-5000 Diffractometer with monochromatic Mo $K\alpha$ radiation ($\alpha=0.07093$ nm). The lattice parameters a and c of prepared pure and lithiated α - Fe_2O_3 samples were determined from the analysis of the X-ray diffraction patterns and are estimated from the formula of a rhombohedral system as shown in Eqn.1.

$$\frac{1}{d^2} = \frac{(h^2+k^2+l^2)\sin 2\alpha + 2(\cos 2\alpha - \cos \alpha)}{a^2 - (1-3\cos 2\alpha + 2\cos 3\alpha)} \quad (1)$$

Where α is the angle between to faces.

The average grain size is calculated employing Scherrer's equation,

$$D = \frac{0.94\lambda}{\beta \cos \theta} \quad (2)$$

Where D is crystallite size, λ is wavelength of X-ray, β is full width at half maximum in radian, and θ is Bragg angle.

The morphologies of samples were investigated by transmission electron microscopy (TEM) (FEI, TECNAI G² 20, TWIN) operating at 200 kV, equipped with a GATAN CCD camera. Mössbauer spectra were recorded at room temperature in a transmission geometry using a conventional ⁵⁷Fe Mössbauer spectrometer employing a 50 mCi ⁵⁷Co/Rh source. The spectra were analyzed using least squares method assuming Lorentzian line shapes. The isomer shift (IS) values are relative to α -Fe at room temperature. The BET surface areas were measured with an Autosorb-iQ and ASiQWiN device from Quantachrome. Specific surface areas were calculated using the BET (Brunauer-Emmett-Teller) method. The IR spectra were taken using NICOLET-6700 Spectrometer. The chemical states of the samples were analyzed by XPS using a Thermo-VG Scientific ESCALab 250 microprobe with a monochromatic Al $K\alpha$ X-ray source (1486.6 eV)

and a typical energy resolution of 0.4–0.5 eV at full width at half maximum (FWHM). The fluoride adsorption experiments were carried out taking 50 mL of solution containing different concentrations of fluoride (10 to 125 mgL^{-1}). The contents were shaken in a horizontal shaker for 24 h at desired pH values. The fluoride concentrations in the remaining solutions were measured with a specific ion electrode (ELIT-8221) by using total ionic strength adjustment buffer (TISAB) solution to eliminate the interference of complexing ions at WATLAB, University of Waterloo. A VERSALAB- Cryo-free vibrating sample magnetometer (VSM) from Quantum Design was used to study magnetic behavior at room temperature (RT). The VSM measurements were performed with sweep magnetic field applying 2.8 T in either direction. About 5 mg of samples were wrapped in Teflon tape for VSM measurement.

Results and discussion

The pure, annealed at 400°C, and at 500°C iron oxide samples without lithium have been coded as FeLi-0 (precursor), FeLi-0a and FeLi-0b (Table S₂) respectively. The sample synthesized in presence of lithium under similar conditions is coded as FeLi-1 while FeLi-2 and FeLi-3 samples were obtained by calcination of FeLi-1 at 400°C and 500°C respectively. On calcination of lithium doped samples, a slight increase in weight % of Fe and Li was observed (Table S₂) due to transformation of some goethite to hematite and conversion of lithium hydroxide to lithium Oxide (the dehydration of LiOH into Li₂O starts at ~ 427°C).⁴¹

Effect of Li concentration: particle size and growth. To explore the role of Li in precipitation reaction, we have carried out the synthesis of iron oxide nanoparticles using a fixed ratio of EGME to Fe(III) (EGME: Fe(III) = 1:6) at different concentrations of Li, and at temperatures in the range of 35 to 100°C. Figures 1a and 1b corresponded to UV-Vis spectra of samples obtained at different Li concentrations and temperatures respectively. The shifting in absorption intensity may correlate to the size of the particle in the solution as for the nanocrystal sol, the absorption intensity shifted to longer wavelength as the particle size increases and vice versa⁴²⁻⁴⁴.

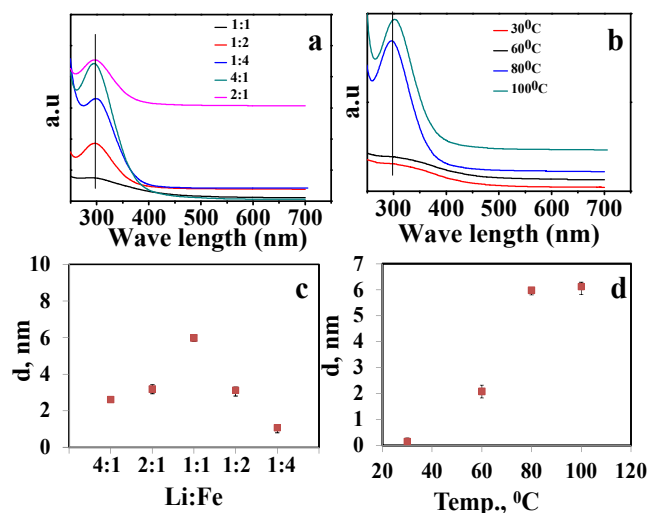


Figure 1. UV-visible absorbance spectra for samples obtained at (a) 80°C using different ratios of Li:Fe, and (b) different temperatures using Li:Fe ratio 1:1. Figs 1(c) and 1(d) represent the average particle sizes of the samples obtained from particle size analyser.

Effects of above mentioned two variables on particle size estimated from particle size analyser are given in Figs 1c and 1d respectively. The growth of iron oxide nanoparticles rapidly decreased with an increase/decrease in the Li concentration on either sides of Li:Fe ratio of 1:1. However, slight increase in particle size was observed at higher temperature. The contents obtained at Li:Fe > 1:1 were gel like. Therefore, the critical concentration ratio of Li: Fe is considered as 1:1.

X-ray diffraction studies. The X-ray diffraction patterns of various samples are given in Figure 2a. The sample FeLi-0 showed characteristic peaks of ferrihydrite and goethite (α -FeOOH). The broad peaks corresponding to (110), (121), (151) and (242) planes of goethite phase are observed (ICDD file Card No. 03-0249). The ferrihydrite phase was confirmed by the presence of peaks corresponding to the (110), (113), (114), (115) and (106) planes (JCPDS card no. 29-0712). Thus the FeLi-0 is a mixture of goethite and ferrihydrite. The XRD pattern of annealed (400°C) sample namely, FeLi-0a was matched to goethite and hematite phases whereas that of FeLi-0b indicated presence of hematite as the only crystalline phase. The XRD patterns of Li doped as synthesized sample (FeLi-1) confirmed formation of crystalline hematite (α -Fe₂O₃) with the peaks corresponding to d-values for rhombohedral structure (ICDD: 00-024-0072). Though XRD of FeLi-1 did not show any ferrihydrite peaks, Mössbauer confirmed presence of this phase (discussed in Mossbauer section). One could also observe peaks corresponding to goethite planes in sample FeLi-2; this indicated that a temperature of 400°C was not adequate for complete transformation of ferrihydrite into hematite as a part of ferrihydrite got transformed to goethite. Formation of pure hematite was observed for sample FeLi-2. In an earlier work, it has been reported that when LiOH is used as a precipitant in place of NaOH, formation of a ferromagnetic precipitate of LiFe₅O₈ took place in alkaline medium at 50°C regardless of the kind of acid anion.⁴⁵ In the present study formation of no such compound was observed. On comparing the % relative intensities (RI) of the synthesized samples with those of standard JCPDS data, it is observed that the % RI of various planes significantly change (supporting Table S₃ (a)). Increase in %RI for (110) plane has been reported in case of plate like α -Fe₂O₃ mesocrystal sample.⁴⁶ Such a phenomena has been explained on the basis of high density of atomic steps, edges, and kinks of such planes.⁴⁵ For the samples under the present study, all the peaks showed shifts which increased with increase in calcination temperature might be due to topotactic incorporation of surface Li ion in hematite matrix. The lattice parameters (Table S₃(b)) decreased along 'a' and 'c' axis for the sample annealed at 500°C (FeLi-3). The cell volume marginally decreased from as synthesized to annealed samples. In general, occupation of Li⁺ in interstitial positions would cause reduction of Fe³⁺. The decrease in unit cell volume upon Li intercalation has been noted previously by Moore et al.⁴⁷ It was explained that Li⁺ ions were not centrally placed on their octahedral sites of α -Fe₂O₃ but the lithium ion was closer to three of the oxygen atoms forming the coordinating octahedron. This may be the reason for decrease in cell volume as for the present samples Fe²⁺ was not observed. In the present study, it can be assumed that lithium was initially adsorbed on the surface of the sample. During calcination the lithium gradually diffused in to the lattice through anionic coordination and on further heating, it gets incorporated/ intercalated in the defect sites of hematite during crystal growth as shown in graphical representation (Figure 2b).

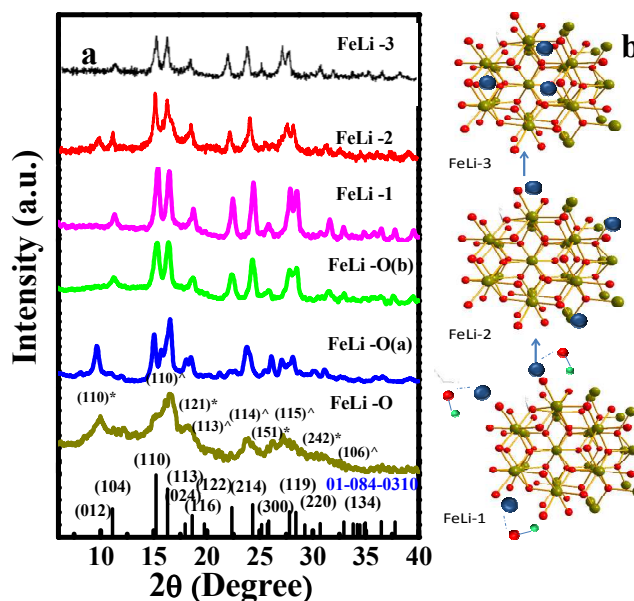


Figure 2 XRD patterns of synthesized iron oxide samples and schematic mechanism of lithium insertion in matrix. ●Li ion, ● Fe ion, ● OH ion. * α -FeOOH phase, ^ ferrihydrite phase.

TEM studies. The TEM images and lattice fringes/selected area electron diffraction (SAED) patterns of iron oxide samples namely FeLi-0, FeLi-0a, FeLi-0b are shown in Figure 3. The sample obtained without Li consists mainly of agglomerated nano particles. The average particle size of 2-5 nm (particles shown in encircled area) was calculated during TEM measurement by magnifying the encircled area (e.g. Figure S₂). Very few thorny extensions of outer surfaces are also observed in some aggregated spherical bundles of nano particles. SAED pattern shows ferrihydrite and goethite Debye-Scherrer rings. TEM of the calcined product of the sample at 400°C has shown more sharp features as compared to original one where as the sample heated at 500°C shows the self-assembled fussy flowery shape is completely disturbed and irregular bundles of nanoparticles with more or less spherical assembly are clearly visible. The TEM images of lithiated samples namely FeLi-1, FeLi-2 and FeLi-3 are given in Figures 4a, 4b and 4c respectively. In presence of lithium, the porous flower-like or urchin-like morphologies are clearly observed. Small petals like extensions which actually overlapped on a number of small rods in a flowery fashion are visible. The SAED pattern showed planes of hematite and ferrihydrite (Figure 4a). For sample FeLi-2, the flower like iron oxide nanostructures for Li doped sample are composed of a number of small rods in a flowery fashion. The microstructure of the sample obtained at 500°C (FeLi-3) showed that the flowers have broken into smaller particles in the range of 10-50 nm with pseudo ellipsoid and pseudo-hexagonal shapes. The particles also showed secondary development of small random tiny particles over bigger particle as base. To get an insight into the growth and self-assembly of nano particles two intermediate samples obtained by keeping the reaction time as 1h (FeLi-1a) and 2h (FeLi-1b) under similar condition were examined. TEM of the sample calcined at 400°C (FeLi-0a) has shown more. From the TEM picture, it is confirmed that initially a large number of nanoparticles are formed at 1 h (Figure 4d), and then their aggregation and iso-oriented fusion in 1D direction to rod shape takes place at 2h (Figure 4e). The sample synthesized at 3h (Figure 4c) showed small petals like

extensions for flowery shaped nanoparticles. The formation process of flowery shaped particles with progress of time may be due to the ligation behavior of EGME which slowed the crystallization process and orientation of the particle in a well defined way.

During the synthesis process, EGME must have played important role in the generation of assembling structure. The interaction of EGME was investigated by UV/Vis analysis and the spectra of precursor solutions with and without EGME were shown in supporting Figure S₁. A strong absorption band appeared around 255 nm. It is proposed that due to ligation, the immediate hydrolysis of iron ion in presence of LiOH is slowed. Since the two dimensional and single-crystalline nanostructures were associated with specific interactions of EGME molecules, the crystal growth could be regarded as ligand-cooperative morphogenesis. The ligand itself and/or Fe³⁺-Li complex along with Li⁺ ion from the basic reagent which interacted with a specific crystal

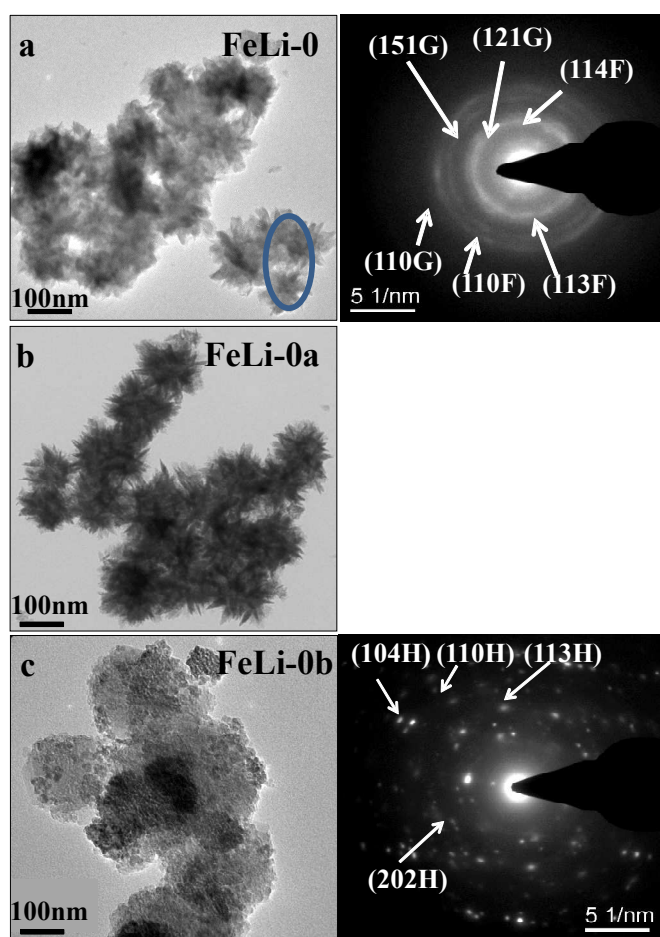


Figure 3 TEM images of iron oxide nano-flower-like structures synthesized without lithium addition (a) FeLi-0, (b) FeLi-0a, (c) FeLi-0b. H =hematite, F= ferrihydrite, G=Goethite

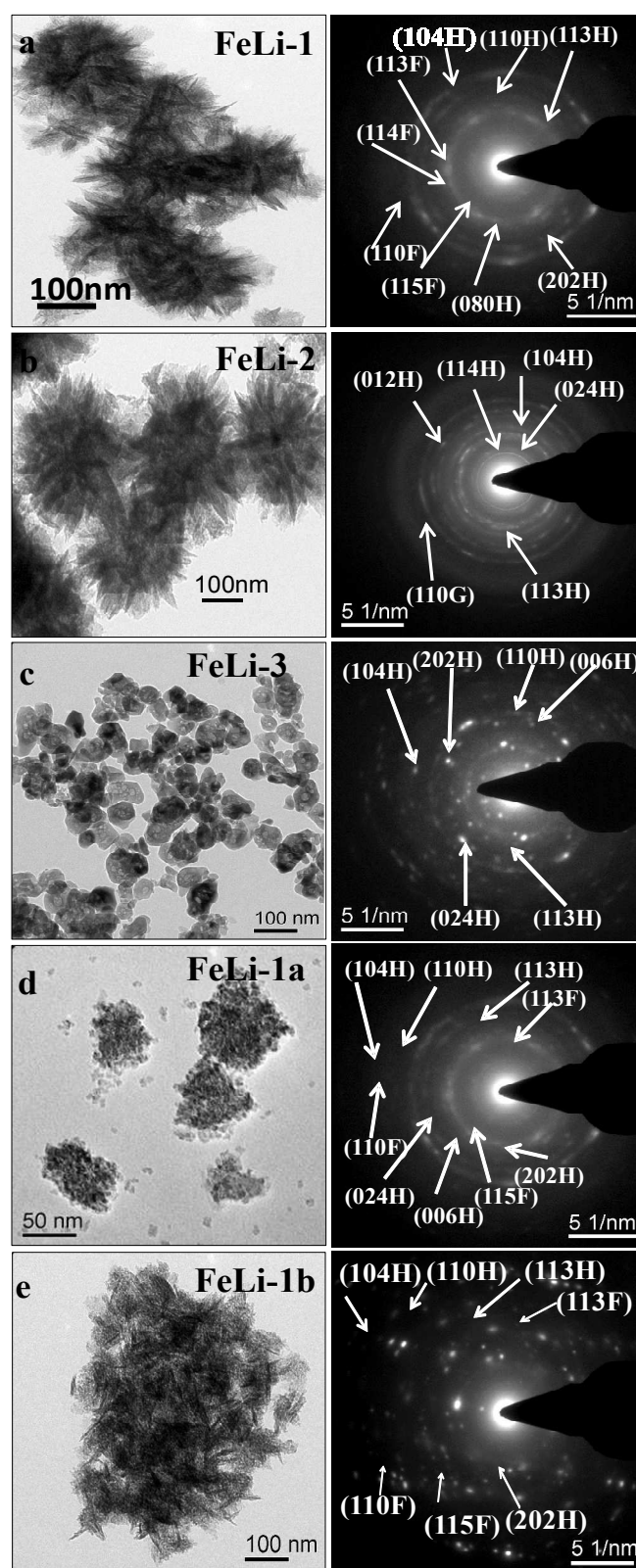


Figure 4. TEM images of iron oxide nano-flower-like structures synthesized with lithium addition (a) FeLi-1obtained at 3h (b) FeLi-2 and (c) FeLi-3, (d) FeLi-1a obtained at 1h, and (e) FeLi-1b obtained at 2 h. H =hematite, F= ferrihydrite, G=Goethite (SAED shows ferrihydrite and goethite Debye-Scherrer rings).

surface and hence contributing to the formation of two-dimensional morphologies with incorporation of lithium through specific interaction. A schematic development and growth of nano flowers α -Fe₂O₃ based iron oxide is tentatively proposed, in Figure 5.

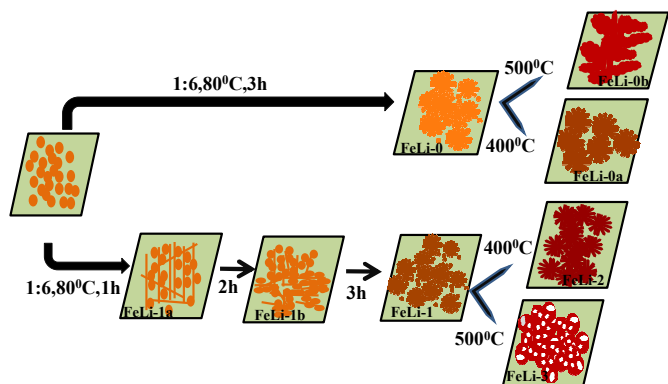


Figure 5. Schematic illustration of the growth model of iron oxide nano-flower like structure and porous hematite.

Mössbauer studies. Mössbauer spectra of the iron oxides samples are shown in Figure 6a. The Mössbauer parameters are given in supporting Table S₄. Spectrum of FeLi-0 showed a combination of a singlet and a doublet corresponding to ferric state only. The Mössbauer parameters of the singlet corresponded to goethite (α -FeOOH) and that of doublet to ferrihydrite. From the relative area of the two components, it was observed that the sample contained about 90% ferrihydrite while rest was goethite. However, the phase formation has been changed completely in the presence of Li under similar conditions. Sample FeLi-1 showed almost equal proportion of ferrihydrite (a doublet of about 52 % area) and hematite (a sextet with about 48 % of area) at room temperature. It may be mentioned here that ferrihydrite phase was not identified in the XRD pattern. The Mössbauer parameters of ferrihydrite formed in FeLi-0 and FeLi-1 samples were similar. This indicated that presence of Li facilitated the transformation of ferrihydrite to hematite. It is also observed that the Mössbauer line width of hematite was relatively very high and have low hyperfine field. It could be because of non-stoichiometric hematite or different type of iron environment seen in the vicinity of probe iron atom. The Mössbauer spectrum of FeLi-2 sample shows ~90 % hematite with ~10% goethite phase. Formation of goethite with annealing is expected due to transformation of ferrihydrite to goethite. The Mössbauer spectrum and parameters of FeLi-3 showed complete transformation of ferrihydrite to hematite. Further studies were focused on lithium doped as synthesized and annealed samples. The samples are analyzed through IR and XPS for the phase and chemical state of the different metal ions (details are given in supporting data along with Figures S₃ and S₄ respectively).

Surface area measurement. The surface area and pore size distribution of flowery shape α -Fe₂O₃ based nanostructures were calculated through nitrogen adsorption-desorption measurement. The Brunauer–Emmett–Teller (BET) surface area of FeLi-1 was estimated as 121.6m²/g from isotherm which is comparable to that reported for mesoporous flowery shape α -Fe₂O₃ (107-130 m² g⁻¹).^{12, 17, 21, 48} In case of FeLi-1 sample, characteristics type IV isotherm (Figure 6b) with type H3 distinct and broad hysteresis loop was observed at a relative pressure P/P₀ of 0.4 to 1. It may be associated

with aggregates of thorny like particles forming slit like pores. Based on the BJH calculation, the pore size distributions of FeLi-1 (Inset Figure 6b) displayed a sharp distribution peak centered at 19.13 nm indicating homogeneity of the pores. These pores were arisen due to void space generated during oriented organization of nanocrystals. In contrast, the more flowery like structure-like nano architecture FeLi-2 showed a relatively low surface area 33.0 m²g⁻¹ and small absorbance of N₂ (Figure 6c) with a typical H3-type hysteresis loop at a relative pressure P/P₀ of 0.9 to 1.0. The shifting of relative pressure towards high value suggests that the pore distribution might originate from the holes between compactly packed primary nano crystals, and the large mesoporous distribution or might originate from some vacancies caused by the absence of subunits.¹³ However, almost same pore-size distribution of 19.12 nm was observed from the BJH analysis (Inset Figure 6c), indicating that small pores exist in both the nanostructures. The collapse of the porous structure during the process of calcination is a general trend and thus cause increase in pore size distribution, which is not observed in our case. The characteristic N₂ adsorption-desorption isotherms and pore size distributions revealed that both the samples have mesoporous structures. FeLi-3 has shown lowest specific surface area of 22.1 m² g⁻¹ and has broad H3-type hysteresis loop as compared to that of FeLi-2 at a relative pressure P/P₀ of 0.75 to 1.0. The BJH analyses showed that the sample possessed bimodal (small and large) mesoporous distribution having main pore size of 19.3nm and in the range of 49-63 nm. By comparing the pore size distribution of 8FeLi-3 with TEM we have concluded that the range of pores with a maximum at around 49-63 nm corresponds to the interspace between individual nanoparticles in agglomerates, and the pore at 19.3 nm corresponds to small pores within individual nanoparticles.

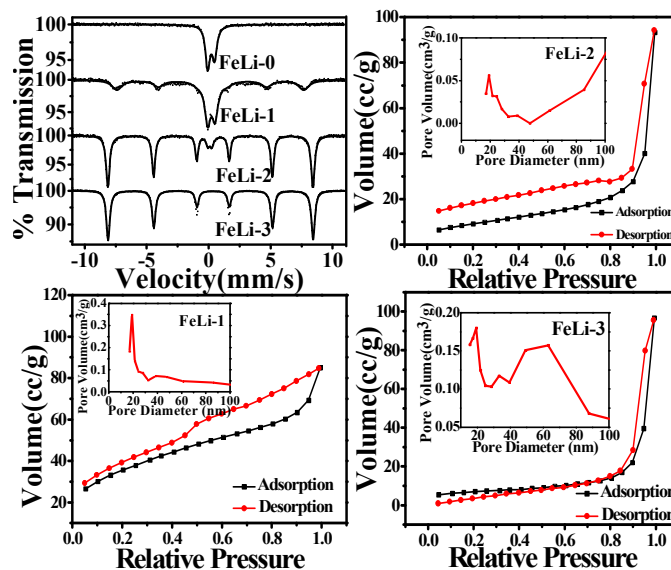


Figure 6a. Mössbauer spectra of synthesized iron oxide samples. (b-d) Nitrogen adsorption-desorption isotherm for lithiated iron oxide samples along with pore size distribution curve as insets, demonstrating the porous structure with high surface area.

Fluoride adsorption properties of Li- doped synthesized samples.

Removal of fluoride for environmental issue has been extensively studied through adsorption process. Depending on the chemistry of solid adsorbent, the adsorption capacities varied. Mainly pH, and surface charges are effective parameters to alter the adsorption

capacity. In general, the more positive the surface is, the better the sorption will be for negatively charged ions. Thus presence of chemical functional groups, metal ions, and anions influence the fluoride binding with adsorbents.^{49,50} The adsorption kinetics of fluoride adsorbed onto pure and lithiated iron oxide nanoparticles and their annealed products were studied at initial fluoride concentrations of 10 mgL⁻¹. The experimental results showed that the equilibrium is reached at 4 h of contact time (Figure 7a). To ensure complete equilibrium the experiments were done at 24 h. It is observed that the pure iron oxide sample has lower adsorption capacity when compared to the lithiated samples. Removals of fluoride ion by as prepared and annealed samples were evaluated using different values of pH (3-12) and are given in Figure 7b. It was seen that the fluoride adsorption efficiency increased with increased solution pH, and decreased at high alkaline range and the trend was coherent with the reported results.⁴⁹⁻⁵¹ However, the pH range for maximum removal of fluoride becomes wider for the annealed samples. It showed the applicability of annealed samples for fluoride adsorption in a broader range of pH. Though the adsorption capacity for as prepared sample was higher than the annealed sample at acidic to neutral pH, but at the alkaline pH the annealed sample showed better adsorption capacities. Highest removal level was observed at pH 6.5- 7.0 for FeLi-1 and a wide pH range 6-9 for both FeLi-2 and FeLi-3 samples. Slight positive pH shift for obtaining highest adsorption of fluoride was observed for the annealed sample. This was due to difference in pHPZC of the sample as shown in Table S₂. The FeLi-2 sample has higher pHPZC than the FeLi-1. Equilibrium adsorption data was generated by variation of initial fluoride concentration at individual pH of maximum adsorption for each sample and the results are shown in Figure 7c. It was observed that the adsorption capacity increased till initial F-concentration of 120 mgL⁻¹ and then saturated. Maximum adsorption capacities of ~99, ~95 and ~91 mgg⁻¹ F⁻ were obtained experimentally for FeLi-1, FeLi-2 and FeLi-3 samples respectively. We next decided to check the applicability of the Langmuir and Freundlich models. The linearized forms of Langmuir and Freundlich isotherms are given in Eq.3 and Eq.4 respectively.

$$\frac{C_e}{q_e} = \frac{1}{q_m b} + \frac{C_e}{q_m} \quad (3)$$

$$\ln q_e = \ln K_F + \frac{1}{n} \ln C_e \quad (4)$$

Where C_e is equilibrium concentration (mgL⁻¹), q_e is the amount adsorbed at equilibrium (mg g⁻¹), q_m is maximum adsorption capacity (mg g⁻¹) for Langmuir isotherms and 'b' (L mg⁻¹) is an energy term which varies as a function of surface coverage strictly due to variations in the heat of adsorption. K_F (Lg⁻¹) and $1/n$ are the Freundlich constants. Parameters for Langmuir and Freundlich models were estimated from plots for C_e/q_e vs. C_e and $\ln q_e$ vs. $\ln C_e$ respectively (supporting Figures 5a and 5b). Langmuir monolayer capacities have derived as ~151.5, ~113 and ~111 mgg⁻¹ F⁻ for FeLi-1, FeLi-2 and FeLi-3 samples respectively. However based on the correlation coefficient values of both the isotherm, the adsorption data showed better fit to Freundlich Model ($R^2 = 0.98-0.99$) when compared to Langmuir model ($r^2 = 0.94-0.96$). This suggested that the multilayer adsorption occurs on heterogeneous surfaces. The stronger binding sites were first occupied by the adsorbates. The binding strength gradually decreased with increasing the occupied sites.⁵¹ The parameters are given in Table S₅.

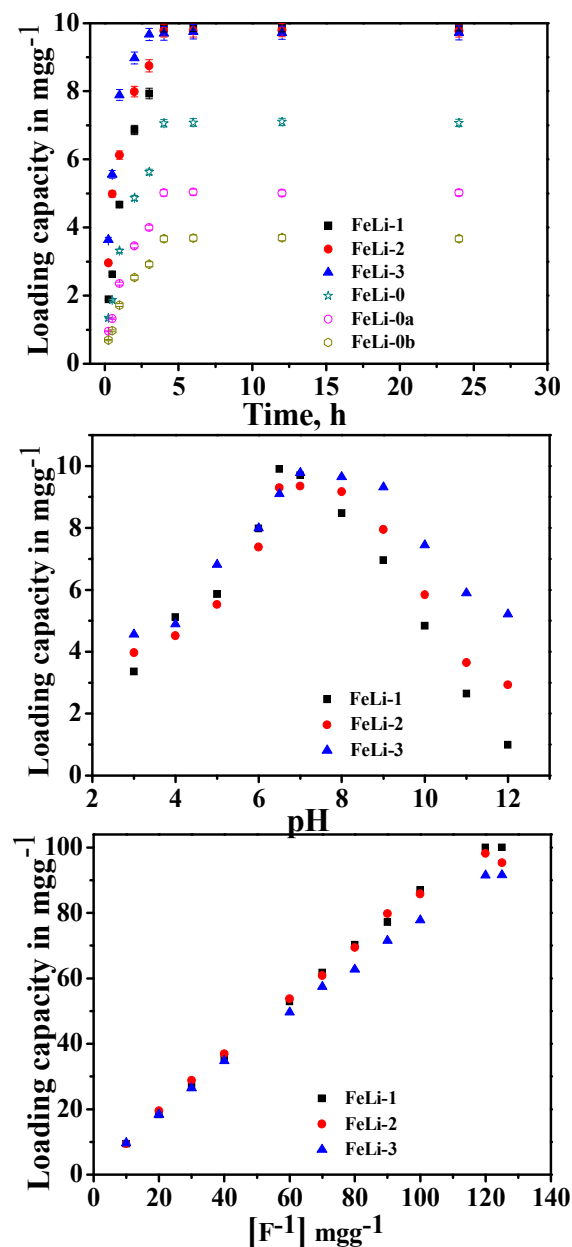


Figure 7(a). Effect of contact time on F⁻ adsorption. Conditions: adsorbent dose 2gL⁻¹, initial F⁻ concentration 10 mgL⁻¹, temperature 30°C, pH 7, **(b)** Effect of solution pH on F⁻ removal contact time 24 h, adsorbent dose 2 gL⁻¹, pH 7, temp. 30°C, and **(c)** Effect of initial F⁻ concentration on its adsorption, adsorbent dose 2gL⁻¹, initial F⁻ concentration 10 mg L⁻¹, temp. 30°C, time 24 h.

Magnetic properties. Moment (M) versus applied field (H) plots for all the samples are shown in Figure 8. It is clear from the plot, that none of the samples saturates even at a maximum applied field of 2.8T. The results can be interpreted on the basis of the field induced diffusion hypothesis.⁵² Defects raised due to sub lattices imbalance would be pushed into the adequately oriented sub lattice by the local magnetic field. The local energy barrier that a defect overcomes to leave its initial position and jump onto the opposite sub lattice is in fact independent (thus possibly much lower) from the energy barrier

of the backward jump. The actual nature of the defects involved, such as vacancies and $\text{Fe}^{2+}/\text{Fe}^{3+}$ linked to the replacement of OH by H_2O remains to be determined, but they are clearly not linked to substitution of iron by other elements in the case of pure iron oxide. Electron-exchange among a Fe^{3+} metal ion, or proton exchange between OH and H_2O may be in the right energy range for field-induced diffusion.⁵² It was observed that as prepared samples FeLi-0 and FeLi-1 are showing maximum magnetization 1.0 and 1.2 emu g^{-1} respectively. This value was close to the value of saturation magnetization of poorly crystalline hematite or ferrihydrite as reported by Bodker et al.⁵³ On heating the FeLi-0 sample at 400°C (sample FeLi-0a) and at 500°C (sample FeLi-0b) maximum magnetization decreased to 0.54 emu g^{-1} which was very close to the reported value of saturation magnetization of hematite nanoparticles (0.4 emu/g).⁵³ The reduction in the maximum magnetization value indicates that calcination leads to formation of hematite in good crystalline phase as discussed in XRD and Mössbauer sections. FeLi-0b sample displayed a relatively bigger hysteresis with coercivity (H_c) of 1898 Oe, which is almost double than that of FeLi-0a (953 Oe, Figure 8). The remnant magnetization (H_r) of FeLi-0b is $0.0428 \text{ emu g}^{-1}$, which is quite higher as compared to that of FeLi-0 ($0.0028 \text{ emu g}^{-1}$). The remanent magnetization and coercive field in the ferrihydrite dominated samples (FeLi-0) was quite low as compared to the annealed samples suggesting that ferrihydrite is magnetically soft material and not much energy has been lost during magnetization de-magnetization process. Whereas, in the hematite dominated sample (FeLi-0a) remanent magnetization and coercive fields were quite high suggesting that the motion of magnetic domain walls became more difficult and much more energy has been lost during magnetization de-magnetization process. As the crystalline fraction increases due to annealing, the maximum value of the coercivity increases due to the stronger interaction between the particles.⁵⁴ Increase in coercivity value was also related to positional randomness of dipolar particle or the clustering of magnetic dipoles.⁵⁵

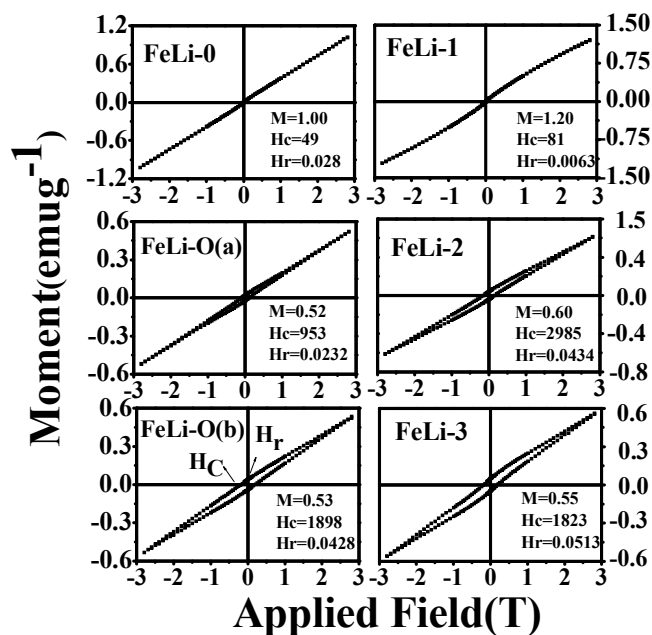


Figure 8. Magnetic hysteresis loops of pure and lithiated iron oxide precursor and their annealed product. Maximum M in (emu/g), H_c (Oe), H_r in emu/g .

In lithiated iron oxide sample, coercivity values increased as compared to pure one. On annealing (400°C) this value (for FeLi-2) is highly increased as compared to that of FeLi-0a. The higher remanent magnetization and coercivity observed in the present study is due to assembly of $\alpha\text{-Fe}_2\text{O}_3$ nanorods to flowery superstructures in presence of lithium. Self-assembling or hierarchical of nano particle causes increase of the magnetic surface anisotropy compared with individual nanorods, which prevents them from being magnetized in directions other than along their easy magnetic axes,⁵⁶ hence leading to the higher remanent magnetization and higher coercivity. Again, the grain size⁵⁷ annealing and the degree of cation substitution (or vacancies) have also controlled the coercivity value. The coercivity of fine-grained hematite was strongly affected by aluminous substitution.⁵⁸⁻⁶⁰ It was reported that the coercivity of hematite increased steadily and non-linearly by increasing aluminum substitution. This was explained on the basis of development of lattice defects⁶⁰ and an increase in the number of the particle crystallites by shrinking the mean crystallite dimensions. Similar behavior has been observed in Sample FeLi-2 where Li-substitution/intercalation may stabilize the domain and increase coercivity. On annealing at 500°C , the flowery shaped structure breaks and smaller particles are formed which should result in increase in coercivity. However, reverse trend was observed. We believed that the low coercivity in FeLi-3 may be due to the larger contribution of surface crystalline defects which are created when lithium tends to diffuse out from the grain boundary of hematite matrix forming solid solution.

Conclusions

In summary, pure/lithium incorporated Fe_2O_3 self-assembled flowery structured samples have been successfully synthesized through a selective ligand mediation process. The main finding of this work is that the ligand coordinated iron complex has been found to play an important role in the orientation of particles. The ligation behaviour of EGME slowed the hydrolysis process and thus the orientation of particles in a well-defined way and played a vital role for self-assembling of nano flower as well as the formation of porous structure. Experimental results on the lithium variation indicate a strong correlation between concentration of lithium and temperature with the particle growth of iron oxide phase which rapidly decreased with an increase in the LiOH concentration beyond a critical concentration. The Mössbauer parameters indicated that presence of Li facilitated the transformation of ferrihydrite to hematite rather than to goethite and hence led to formation of hematite at room temperature. Adsorption performances of the samples were evaluated. Maximum experimental adsorption capacities of ~ 99 , ~ 95 and $\sim 91 \text{ mg g}^{-1} \text{ F}^-$ were obtained for FeLi-1, FeLi-2 and FeLi-3 samples respectively. Whereas the Langmuir monolayer capacities for them have derived as ~ 151.5 , ~ 113 and $\sim 111 \text{ mg g}^{-1} \text{ F}^-$ respectively. Magnetization measurements suggested that the coercivity values were evidently improved by annealing of pure iron oxides where as in case of lithiated sample this value increased on annealing at 400°C and decreased for the sample obtained on annealing at 500°C . The low coercivity value indicated the role of lithium in creating surface crystalline defects. However, this unusual magnetic behaviour needs further study for deep understanding of mechanism. The formation of the nano flowers through the present route provides a strategy for synthesising other functional materials. The surface properties of the synthesized samples in terms of adsorption and their interesting magnetic behaviour evidently shows that the samples can be expected their utilisation in advance field of application.

Acknowledgements

This work is supported by the DST, India (Inspire Fellowship Program). The author, Dr. M. Mohapatra is also thankful to DST for providing BOYSCAST fellowship. The Authors are thankful to Prof. B.K. Mishra, Director, Institute of Minerals and Materials Technology, Bhubaneswar for his kind permission to publish this paper. We are very much thankful to Prof. K.T. Leung, Director WATLAB, University of Waterloo and N. Moghimi, PhD student, University of Waterloo for carrying out XPS characterization and also thankful to Dr I. N. Bhattacharya (H.O.D) and Dr T. Subbaiah (chief scientist) of Hydro-electro Metallurgy Department, IMMT, Bhubaneswar.

Notes and references

^a Institute of Minerals and Materials Technology, Bhubaneswar-751015, Odisha, India

^b Department of Applied Science, Symbiosis Institute of Technology, Mulsi, Pune 412 115, India Address here.

Electronic Supplementary Information (ESI) available: [details of any supplementary information available should be included here]. See DOI: 10.1039/b000000x/

References

- 1 Y. Yang, H. X. Ma, J. Zhuang and X. Wang, *Inorg. Chem.*, 2011, **50**, 10143-10151.
- 2 Y. C. Ling, G. M. Wang, D. A. Wheeler, J. Z. Zhang and Y. Li, *Nano Lett.*, 2011, **11**, 2119-2125.
- 3 L. Vayssieres, N. Beermann, S. E. Lindquist and A. Hagfeldt, *Chem. Mater.*, 2001, **13**, 233-235.
- 4 R. Wang, Y. Chen, Y. Fu, H. Zhang and C. Kisielowski, *J. Phys. Chem. B*, 2005, **109**, 12245-12249.
- 5 C. J. Jia, L. D. Sun, Z. G. Yan, L. P. You, F. Luo, X. D. Han, Y. C. Pang, Z. Zhang and C. H. Yan, *Angew. Chem., Int. Ed.*, 2005, **44**, 4328-4333.
- 6 A. Mao, K. Shin, J. K. Kim, D. H. Wang, G. Y. Han and J. H. Park, *ACS Appl. Mater. Interfaces*, 2011, **3**, 1852-1858.
- 7 W. Wu, X. Xiao, S. Zhang, J. Zhou, L. Fan, F. Ren and C. Jiang, *J. Phys. Chem. C*, 2010, **114**, 16092-16103.
- 8 Z. Zhang, M. F. Hossain and T. Takahashi, *Appl. Catal. B*, 2010, **95**, 423-429.
- 9 J. Liu, Y. Li, H. Fan, Z. Zhu, J. Jiang, R. Ding, Y. Hu and X. Huang, *Chem. Mater.*, 2009, **22**, 212-217.
- 10 A. L. Cavalieri, N. Muller, T. Uphues, V. S. Yakovlev, A. Baltuska, B. Horvath, B. Schmidt, L. Blumel, R. Holzwarth, S. Hendel, M. Drescher, U. Kleineberg, P. M. Echenique, R. Kienberger, F. Krausz and U. Heinzmann, *Nature*, 2007, **449**, 1029-1032.
- 11 H. M. Fan, G. J. You, Y. Li, Z. Zheng, H. R. Tan, Z. X. Shen, S. H. Tang and Y. P. Feng, *J. Phys. Chem. C*, 2009, **113**, 9928-9935.
- 12 L. L. Wang, T. Fei, Z. Lou and T. Zhang, *Appl. Mater. Interfaces*, 2011, **12**, 4689-4694.
- 13 X. L. Fang, C. Chen, M. S. Jin, Q. Kuang, Z. X. Xie, S. Y. Xie, R. B. Huang and L. S. Zheng, *J. Mater. Chem.*, 2009, **19**, 6154-6160.
- 14 L. Wang and L. Gao, *J. Am. Ceram. Soc.*, 2008, **10**, 3391-3395.
- 15 Q. Hao, S. Liu, X. Yin, Z. Du, M. Zhang, L. Li, Y. Wang, T. Wang and Q. Li, *Cryst. Eng. Comm.*, 2011, **13**, 806-812.
- 16 S. Y. Zeng, K. B. Tang, T. W. Li, Z. H. Liang, D. Wang, Y. K. Wang, Y. X. Qi and W. W. Zhou, *J. Phys. Chem. C*, 2008, **112**, 4836-4843.
- 17 W. Zhou, L. Lin, W. Wang, L. Zhang, Q. Wu, J. Li, and L. Guo, *J. Phys. Chem. C*, 2011, **115**, 7126-7133.
- 18 X. L. Cheng, J. S. Jiang, M. Hu, G. Y. Mao, F. X. Bu, C. C. Lin, Y. Zeng and Q. H. Zhang, *Cryst. Eng. Comm.*, 2012, **14**, 7701-7708.
- 19 X. Liu, J. Guo, Y. Cheng, Y. Li, G. Xu and P. Cui, *J. Cryst. Growth*, 2008, **311**, 147-151.
- 20 X. Mou, X. Wei, Y. Li and W. Shen, *Cryst. Eng. Comm.*, 2012, **14**, 5107-5120.
- 21 C. Y. Cao, J. Qu, W. S. Yan, J. F. Zhu, Z. Y. Wu and W. G. Song, *Langmuir*, 2012, **28**, 4573-4579.
- 22 C. Anmin, C. Liangliang and G. Di, *Appl. Phys. Lett.*, 2007, **91**, 034102-034104.
- 23 C. A. Mirkin, R. L. Letsinger, R. C. Mucic and J. J. Storhoff, *Nature*, 1996, **382**, 607-609.
- 24 A. K. Boal, F. Ihan, J. E. DeRouchey, T. T. Abrecht, T. P. Russell and V. M. Rotello, *Nature*, 2000, **404**, 746-748.
- 25 J. Q. Zhuang, H. M. Wu, Y. G. Yang and Y. C. Cao, *Angew. Chem., Int. Ed.*, 2008, **47**, 2208-2212.
- 26 F. Bai, D. S. Wang, Z. Y. Huo, W. Chen, L. P. Liu, X. Liang, C. Chen, X. Wang, Q. Peng and Y. D. Li, *Angew. Chem., Int. Ed.*, 2007, **46**, 6650-6653.
- 27 N. C. Bigall, T. Hartling, M. Klose, P. Simon, L. M. Engand and A. Eychmuller, *Nano Lett.*, 2008, **8**, 4588-4592.
- 28 A. Narayanaswamy, H. F. Xu, N. Pradhan and X. G. Peng, *Angew. Chem., Int. Ed.*, 2006, **45**, 5361-5364.
- 29 T. P. Chou, Q. F. Zhang, G. E. Fryxell and G. Z. Cao, *Adv. Mater.*, 2007, **19**, 2588-2592.
- 30 X. L. Hu, J. M. Gong, L. Z. Zhang and J. C. Yu, *Adv. Mater.*, 2008, **20**, 4845-4850.
- 31 J. S. Hu, L. L. Ren, Y. G. Guo, H. P. Liang, A. M. Cao, L. J. Wan and C. L. Bai, *Angew. Chem., Int. Ed.*, 2005, **44**, 1269-1273.
- 32 G. Liu, Q. Deng, H. Wang, D. H. L. Ng, M. Kong, W. Cai and G. Wang, *J. Mater. Chem.*, 2012, **22**, 9704-9713.
- 33 F. H. Zhang, H. Q. Yang, X. L. Xie, L. Li, L. H. Zhang, J. Yu, H. Zhao and B. Liu, *Sens. Actuators, B*, 2009, **141**, 381-389.
- 34 Q. Y. Hao, S. Liu, X. M. Yin, Z. F. Du, M. Zhang, L. M. Li, Y. G. Wang, T. H. Wang and Q. H. Li, *Cryst. Eng. Comm.*, 2011, **13**, 806-812.
- 35 Y. Han, Y. J. Wang, L. Li, Y. P. Wang, L. F. Jiao, H. T. Yuan and S. X. Liu, *Electrochim. Acta*, 2011, **56**, 3175-3181.
- 36 A. Turkovic, M. Ivanda, M. Bitenc and Z. C. Orel, *J. Nanomaterials*, 2011, AID 967307, **8p**.
- 37 H. Morimoto, S. Tobishima and Y. Iizuka, *J. Power Sources*, 2005, **146**, 315-318.
- 38 B. Koo, H. Xiong, M. D. Slater, V. B. Prakapenka, M. Balasubramanian, P. Podsiadlo, C. S. Johnson, T. Rajh and E. V. Shevchenko, *Nano Lett.* 2012, **12**, 2429-2435.
- 39 D-W. Junga, S-W. Hana, B-S. Kong and E-S Oha, *J. Power Sources*, 2013, **242**, 357-364
- 40 A. I. Vogel, *A Text Book of Quantitative Inorganic Analysis*, English Language 28 Book Society, Longmans Green Publishers, London, 2000.
- 41 J. M. Kiat, G. Boemare, B. Rieuaud and D. Aymes, *Solid State Comm.*, 1998, **108**, 241-245.
- 42 M. Husein, E. Rodil, and J. H. Vera, *Langmuir*, 2003, **19**, 8467-8474.
- 43 E. M. Moreno, M. Zayat, M. P. Morales, C. J. Serna, A. Roig and D. Levy, *Langmuir*, 2002, **18**, 4972-4978.

- 44 K. Cheng, Y. P. He, Y. M. Miao, B. S. Zou, Y. G. Wang, T. H. Wang, X. T. Zhang and Z. L. Du, *J. Phys. Chem. B*, 2006, **110**, 7259-7264.
- 45 M. Kiyam, T. Taka, Bull. Inst. Chem. Res., Kyoto Univ., 1980, **58**, 193-200.
- 46 J. Ma, J. Teo, L. Mei, Z. Zhong, Q. Li, T. Wang, X. Duan, J. Lian and W. Zheng, *J. Mater. Chem.*, 2012, **22**, 11694-1700.
- 47 E. A. Moore, H. M. Widatallah and F. J. Berry, *J. Phys. Chem. Solids*, 2012, **63**, 519-523.
- 48 B. Sun, J. Horvat, H. S. Kim, W-S. Kim, J. Ahn, and G. Wang, *J. Phys. Chem. C*, 2010, **114**, 18753-18761.
- 49 M. Mohapatra, K. Rout, P. Singh, S. Anand, S. Layek, H. C. Verma, and B. K. Mishra, *J. Hazard. Mater.* 2011, **186**, 1751-1757.
- 50 M. Mohapatra, D. Hariprasad, L. Mohapatra, S. Anand and B. K. Mishra, *App. Sur. Sci.*, 2012, **258**, 4228-4236.
- 51 X. Zhao, J. Wang, F. Wu, T. Wang, Y. Cai, Y. Shi and G. Jiang, *J. Hazard Mater.*, 2010, **173**, 102-109.
- 52 P. Rochette, P-E. Mathe, L. Esteban, H. Rakoto, J-L. Bouchez, Q. Liu, and J. Torrent, *Geophysical Research Letters*, 2005, **32**, 1-L22309.4.
- 53 F. Bødker, M. F. Hansen, C. B. Koch, K. Lefmann, and S. Mørup, *Phys. Rev. B*, 2000, **61**, 6826-683.
- 54 V. Franco, L. F. Kiss, T. Kemény, I. Vincze, C. F. Conde, and A. Conde, *Phys. Rev. B*, 2002, **66**, 224418.
- 55 B. Yang and Y. Zhao, *J. appl. Phys.*, 2011, **110**, 103908(7p).
- 56 L-P Zhu, H-M Xiao, X-M Liu and S-Yun Fu, *J. Mater. Chem.*, 2006, **16**, 1794-1797.
- 57 G. Kletetschka and P. J. Wasilewski, *Phys. Earth Planet. Inter.*, 2002, **129**, 173-179.
- 58 Q. S. Liu, A. P. Roberts, J. Torrent, C. S. Horng and J. C. Larrasoana, *Geochem. Geophys. Geosys.*, 2007, **8**, 09011, doi:09010.01029/02007GC001717
- 59 A. P. Roberts, Q. S. Liu, C. J. Rowan, L. Chang, C. Carvallo, J. Torrent, and C. S. Horng, *J. Geophys. Res.*, 2006, **111**, B12S35, doi: 10.1029/2006JB004715.
- 60 M. A. Wells, R.W. Fitzpatrick, R. J. Gilkes and J. Dobson, *Geophys. J. Int.*, 1999, **138**, 571-580.

